# Letters

## Transient Modeling and Postfault Stability Analysis of GFM-DFIG Considering Rotor-Side Current Limitation

Ling Zhan, Bin Hu, *Member, IEEE*, Han Li, Zhijian Zhao, Liang Chen, Heng Nian, *Senior Member, IEEE*, and Donglian Qi, *Senior Member, IEEE*

***Abstract*—This letter establishes transient models of current-limited grid-forming doubly fed induction generator (GFM-DFIG) that incorporate the dynamics of the voltage controller. Based on the switching logic between normal operation and current limitation, the impact of the saturated current angle on the transient performance of the system is revealed. Theoretical analysis and experimental results demonstrate that GFM-DFIG exhibits three distinct transient behaviors after fault clearance, including withdrawal of current limitation, high-frequency oscillations, and remaining locked in saturation, which guide the selection of current limiting parameters.**

***Index Terms*—Current limitation, fault recovery, grid-forming doubly fed induction generator (GFM-DFIG), transient stability.**

### I. Introduction

As THE penetration of renewable energy sources continues to increase, the global installed capacity of wind turbines is experiencing rapid expansion [1], [2]. This paradigm change requires the implementation of grid-forming (GFM) strategies by doubly fed induction generators (DFIGs) to support the frequency and voltage of the power grid [3], [4].

Recently, transient stability of GFM units under large disturbances has received widespread attention. Li et al. [5] analyzed the mechanism by which improper controller parameters lead to transient instability in GFM-DFIG. An improved hybrid synchronization method is then proposed to enhance the stable equilibrium point (SEP) and transient damping of the system. However, the study assumes that the rotor-side current of the DFIG is always within the maximum permissible range, which may lead to an overly optimistic assessment of transient performance.

Due to the voltage source characteristics of GFM-DFIG, it is crucial to select an appropriate current limitation algorithm for protecting the rotor-side converter (RSC) during contingencies. The application of current limiters can effectively restrict fault currents, as the current controllers in GFM devices are typically designed for rapid command tracking [4], [5]. Compared to the circular limiter [4], the priority-based limiter [6], [7] has an additional degree of freedom in the saturated current angle (SCA), allowing for more flexible parameter configurations. Moreover, its ability to adjust the ratio of $dq$-axis current during fault conditions is also recommended by IEEE P2800 [8].

Since the priority-based limiter is consistently triggered during severe faults, further investigation is required to assess whether the system can restore normal operation with guaranteed transient stability after fault clearance. Previous research has conducted extensive studies on the postfault behavior of voltage source converters (VSCs). Huang et al. [6] revealed the instability mechanism of a GFM-VSC equipped with $d$-axis priority-based limiter after fault restoration. Fan and Wang [7] illustrated the impact of short-circuit ratios and current limiter parameters on the fault recovery process of a GFM-VSC. Further efforts focus on optimizing the SCA to increase the critical clearing time of the system [9], and identifies the current saturation procedure in GFM-type IV wind turbines caused by the priority-based limiter [10].

While the above studies provide valuable insights for understanding the impacts of the limiter, the unique characteristics of the DFIG system necessitate a separate investigation. When a priority-based limiter is applied in GFM-DFIG, the main difference lies in that the output of the RSC is the rotor voltage, while it performs the GFM function on the stator side. In other words, an asynchronous machine acts as an intermediary between the control objective and its implementation. This inherent machine dynamics and the coupling between rotor voltage control and stator GFM capability introduce unique challenges compared to VSC implementations. To address this gap, the dynamics of the voltage controller need to be considered to fully analyze the

Received 10 February 2025; revised 13 April 2025; accepted 5 May 2025. Date of publication 9 May 2025; date of current version 30 June 2025. This work was supported in part by the National Natural Science Foundation of China under Grant 52325702 and Grant 52407069, in part by the Science and Technology Project of Zhejiang Province under Grant 2024C01177, in part by the Zhejiang Provincial Natural Science Foundation of China under Grant LMS25E070001, and in part by the China Postdoctoral Science Foundation under Grant 2024T170766 and Grant 2024M762824. *(Corresponding author: Heng Nian.)*

Ling Zhan, Bin Hu, Han Li, Heng Nian, and Donglian Qi are with the College of Electrical Engineering, Zhejiang University, Hangzhou 310027, China (e-mail: zhanling@zju.edu.cn; binhuee@zju.edu.cn; 12110058@zju.edu.cn; nianheng@zju.edu.cn; qidl@zju.edu.cn).

Zhijian Zhao is with Windey Energy Technology Group Company, Ltd., Hangzhou 310013, China (e-mail: zhaozhijian@windeyenergy.com).

Liang Chen is with the School of Information Science and Engineering, NingboTech University, Ningbo 315104, China (e-mail: 21410077@zju.edu.cn).

Color versions of one or more figures in this article are available at https://doi.org/10.1109/TPEL.2025.3568597.

Digital Object Identifier 10.1109/TPEL.2025.3568597

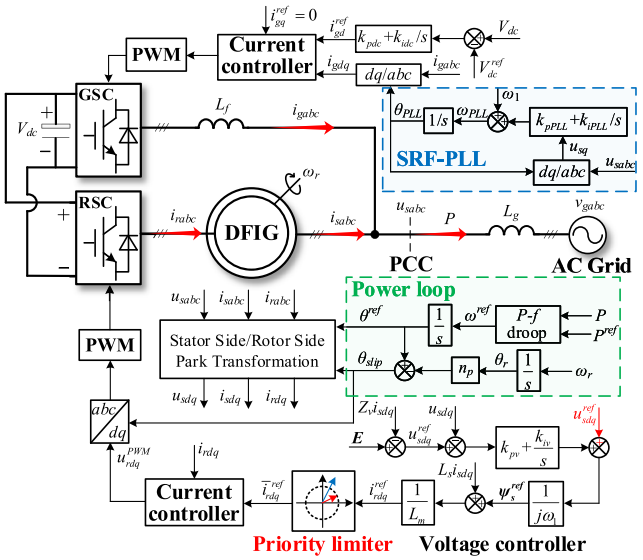


Fig. 1. System block diagram of GFM-DFIG during the transient process.

transient performance of GFM-DFIG, which is fundamentally different from that of a VSC. And the interplay between the generator, the voltage controller, and the current limiter has not been sufficiently studied.

To that end, this letter develops transient models of GFM-DFIG considering rotor-side current limitation under different operating conditions. The postfault behavior of the system under various controller parameters is revealed, which includes withdrawal of current limitation, high-frequency oscillations, and remaining locked in saturation. Finally, theoretical analysis is validated through experimental tests.

## II. Current-Limited GFM-DFIG

Fig. 1 presents the block diagram of a current-limited GFM-DFIG during the transient process. Since the grid-side converter (GSC) operates on a fast time scale with grid-following control, it can promptly transmit the slip power fluctuations from the RSC, ensuring the input–output balance in the dc link. Therefore, this letter simplifies the analysis by replacing the GSC with a constant dc voltage source $V_{\mathrm{dc}}$ [5], [11]. $v_{\mathrm{gabc}}$ and $u_{\mathrm{sabc}}$ represent the grid voltage and stator voltage, respectively, while $i_{\mathrm{sabc}}$ and $i_{\mathrm{rabc}}$ denote the stator and rotor currents. $P$ signifies the active power output. Reference angle $\theta^{\mathrm{ref}}$ and slip angle $\theta_{\mathrm{slip}}$ calculated from the power controller are used for coordinate transformation of stator-side and rotor-side variables, respectively. To achieve the primary objective of voltage restoration after the fault and to ensure a smooth transition of the control strategy, this letter selects a constant voltage magnitude reference to implement reactive power regulation during the transient process [4], [7]. The specific circuit and controller parameters are provided in Table I.

The voltage controller is designed based on the DFIG stator voltage equation in the $dq$-frame. The feedforward from voltage reference $u_{\mathrm{sdq}}^{\mathrm{ref}}$ is added to the proportional-integral (PI) regulator

TABLE I
System and Controller Parameters

| Parameter | Value | Parameter | Value |
|---|---|---|---|
| $V_g$, Grid voltage | 563 V | $\omega_1$, Rated angular frequency | $100\pi$ rad/s |
| $P^{ref}$, Power reference | 2.75 MW | $L_g$, Grid inductance | 0.25 p.u. |
| $K_e$, Turn ratio | 0.35 | $L_s$, Stator inductance | 6.35 p.u. |
| $n_p$, Pairs of poles | 2 | $L_r$, Rotor inductance | 6.53 p.u. |
| $R_s$, Stator resistance | 0.01 p.u. | $L_m$, Magnetizing inductance | 6.17 p.u. |
| $R_r$, Rotor resistance | 0.01 p.u. | $E$, Voltage reference | 1 p.u. |
| $R_v$, Virtual resistance | 0 | $L_v$, Virtual inductance | 0.1 p.u. |
| $K_p$, Droop gain | 0.01 p.u. | $I_{\max}$, Maximum current | 1.5 p.u. |

that eliminates the voltage deviation, and its output represents the reference stator flux linkage $\psi_s^{\mathrm{ref}}$.

After the voltage loop, a commonly utilized priority-based limiter is cascaded to restrict the magnitude of RSC output current, which can be expressed as

$$\bar{i}_{\mathrm{rdq}}^{\mathrm{ref}} = \begin{cases} i_{\mathrm{rdq}}^{\mathrm{ref}} & \left\| i_{\mathrm{rdq}}^{\mathrm{ref}} \right\| \le I_{\max} \\ I_{\max} e^{j\varphi} & \left\| i_{\mathrm{rdq}}^{\mathrm{ref}} \right\| > I_{\max} \end{cases} \tag{1}$$

where $i_{\mathrm{rdq}}^{\mathrm{ref}}$ and $\bar{i}_{\mathrm{rdq}}^{\mathrm{ref}}$ are the outputs of the voltage controller and current limiter, respectively. $\varphi$ denotes the SCA.

For the transient saturation phenomenon that may occur during faults, it is assumed that its impact can be addressed through standard compensation techniques or hardware protection, and the detailed dynamics of these phenomena have a minimal effect on the fault recovery characteristics of GFM-DFIG. Therefore, this letter does not include a detailed model for RSC saturation, which is also a common practice in existing literature on DFIG low voltage ride through [11], [12].

## III. Transient Modeling

While steady-state models, such as the T-equivalent circuit, can represent the DFIG during stable operation, they fail to adequately capture the complex characteristics during transient process, including the interactions between machine dynamics, voltage controllers, and current limiters. Therefore, transient models of GFM-DFIG under both normal operation and current limiting conditions will be established in this section.

During normal operation, the introduction of the feedforward term $u_{\mathrm{sdq}}^{\mathrm{ref}}$ results in the output of the voltage PI regulator being approximately zero, as it merely serves to mitigate the impacts of modeling errors. To prevent wind-up in fault periods, the integral coefficient of the voltage loop is set to zero when the current limiter is triggered [4], [7]. Such a control scheme can reduce the order of the GFM-DFIG transient model and enhance the dynamic response capability of the system [13].

The voltage controller shown in Fig. 1 can be expressed as

$$i_{\mathrm{rdq}}^{\mathrm{ref}} = \frac{\boldsymbol{E} - Z_v i_{\mathrm{sdq}} + k_{pv}\left(\boldsymbol{E} - Z_v i_{\mathrm{sdq}} - u_{\mathrm{sdq}}\right) + j\omega_1 L_s i_{\mathrm{sdq}}}{j\omega_1 L_m} \tag{2}$$

where $Z_v = R_v + j\omega_1 L_v$ represents the virtual impedance.

By combining the stator voltage equation of the DFIG with Kirchhoff's voltage equation for the grid inductance, $u_{\mathrm{sdq}}$ and

$i_{\mathrm{sdq}}$ in (2) can be calculated as follows:

$$\begin{cases} u_{\mathrm{sdq}} = \dfrac{L_s v_{\mathrm{gdq}} + j\omega_1 L_g L_m i_{\mathrm{rdq}}}{L_g + L_s} \\ i_{\mathrm{sdq}} = \dfrac{j v_{\mathrm{gdq}} + \omega_1 L_m i_{\mathrm{rdq}}}{\omega_1 (L_g + L_s)} \end{cases} \tag{3}$$

where $v_{\mathrm{gdq}} = V_g \mathrm{e}^{-j\delta}$, with power angle $\delta$ defined as the phase difference between reference voltage $\boldsymbol{E}$ and grid voltage $v_{\mathrm{gdq}}$.

Since the dominant dynamics of transient stability lie in the low-frequency range at the electromechanical time scale, it can be assumed that the RSC output current can always track the command [5], [13]. Therefore, transient models of GFM-DFIG under different operating conditions can be established.

### A. Normal Operation

When the current limiter is not triggered, $i_{\mathrm{rdq}} = \bar{i}_{\mathrm{rdq}}^{\mathrm{ref}} = i_{\mathrm{rdq}}^{\mathrm{ref}}$ holds. Therefore, substituting (3) into (2), $i_{\mathrm{rdq}}^{\mathrm{ref}}$ can be recalculated as follows:

$$i_{\mathrm{rdq}}^{\mathrm{ref}} = \frac{\omega_1 (L_g + L_s)\boldsymbol{E} - j Z_v v_{\mathrm{gdq}} - \omega_1 L_s v_{\mathrm{gdq}}}{\omega_1 L_m (Z_v + j\omega_1 L_g)}. \tag{4}$$

According to (1), GFM-DFIG transitions from normal operating conditions to current limiting mode, if

$$\delta \in \Omega_1 \triangleq \left\{ \delta' \in \boldsymbol{S} \,\middle|\, \left\| i_{\mathrm{rdq}}^{\mathrm{ref}}(\delta') \right\| > I_{\max} \right\} \tag{5}$$

where the set $\boldsymbol{S}$ denotes the unit circle, and the expression for $i_{\mathrm{rdq}}^{\mathrm{ref}}$ is provided in (4).

### B. Current Limitation

When the priority-based limiter is triggered, the following condition is satisfied:

$$i_{\mathrm{rdq}} = \bar{i}_{\mathrm{rdq}}^{\mathrm{ref}} = I_{\max} e^{j\varphi}. \tag{6}$$

Substituting (3) and (6) into (2), $i_{\mathrm{rdq}}^{\mathrm{ref}}$ can be rewritten as shown in (7), where $\lambda_1$ and $\lambda_2$ are expressed in (8)

$$i_{\mathrm{rdq}}^{\mathrm{ref}} = \frac{\boldsymbol{E} - \lambda_1 - k_{pv}\left( \frac{L_s v_{\mathrm{gdq}} + j\omega_1 L_g L_m I_{\max} e^{j\varphi}}{L_g + L_s} - \boldsymbol{E} + \lambda_1 \right) + \frac{j L_s \lambda_2}{L_g + L_s}}{j\omega_1 L_m} \tag{7}$$

$$\begin{cases} \lambda_1 = \frac{\lambda_2 Z_v}{\omega_1 (L_g + L_s)} \\ \lambda_2 = j v_{\mathrm{gdq}} + \omega_1 L_m I_{\max} e^{j\varphi}. \end{cases} \tag{8}$$

Based on (1), GFM-DFIG switches from current limiting state back to normal operation mode, if

$$\delta \in \Omega_2 \triangleq \left\{ \delta' \in \mathbf{S} \,\middle|\, \left\| i_{\mathrm{rdq}}^{\mathrm{ref}}(\delta') \right\| \le I_{\max} \right\} \tag{9}$$

where the expression for $i_{\mathrm{rdq}}^{\mathrm{ref}}$ is given in (7) and (8).

Combining (3) and (6), active power output of GFM-DFIG in current limiting state can be calculated in (10), with $i_{\mathrm{sdq}}^{*}$ denoting the conjugate of the complex stator current

$$P_{\mathrm{limiting}} = \mathrm{Re}\left\{ u_{\mathrm{sdq}} i_{\mathrm{sdq}}^{*} \right\} = \frac{L_m V_g I_{\max} \cos(\varphi + \delta)}{L_g + L_s}. \tag{10}$$

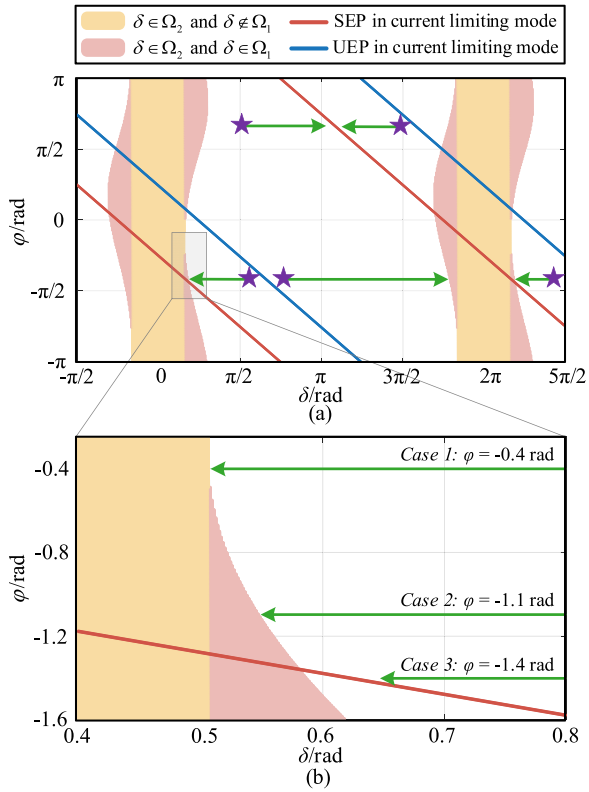


Fig. 2. (a) Transient stability of GFM-DFIG under different SCA selections. (b) Zoomed-in view.

## IV. Transient Stability Analysis

Based on (5), (9), and (10), transient stability of current-limited GFM-DFIG can be analyzed, as shown in Fig. 2(a). Here, the red and blue lines represent the SEPs and unstable equilibrium points (UEPs) of the power angle curves under current limiting state respectively, which vary with the SCA plotted on the $y$-axis. The abscissas of the purple stars represent the positions of operating points at the instant of fault clearance, with green arrows indicating the direction of movement in the subsequent moment. It can be observed that between adjacent SEPs and UEPs, $\delta$ moves to the left after fault recovery since the power angle curve is located above the active power reference. In the remaining regions, $\delta$ moves to the right after fault clearance.

Fig. 2(b) illustrates the specific movement of operating points under different SCA selections. In *Case 1*, $\delta$ moves into the yellow region after fault clearance, indicating $\delta \in \Omega_2$ and $\delta \notin \Omega_1$ holds. Therefore, GFM-DFIG can exit the current limiting state and remain in normal operating condition, when $\varphi = -0.4$ rad is applied. The pink region entered in *Case 2* represents the set $\delta \in \Omega_2 \cap \Omega_1$, indicating that while $\delta \in \Omega_2$ allows GFM-DFIG to restore normal operation, $\delta \in \Omega_1$ causes the output of the voltage controller to trigger the limiter again. As a result, the priority-based limiter introduces high-frequency oscillations in GFM-DFIG due to repeated switching of operating modes. As shown in *Case 3*, when $\varphi = -1.4$ rad is selected, the system stabilizes at a SEP in the current limiting state before reaching the region corresponding to $\Omega_1$ and $\Omega_2$. Consequently, GFM-DFIG

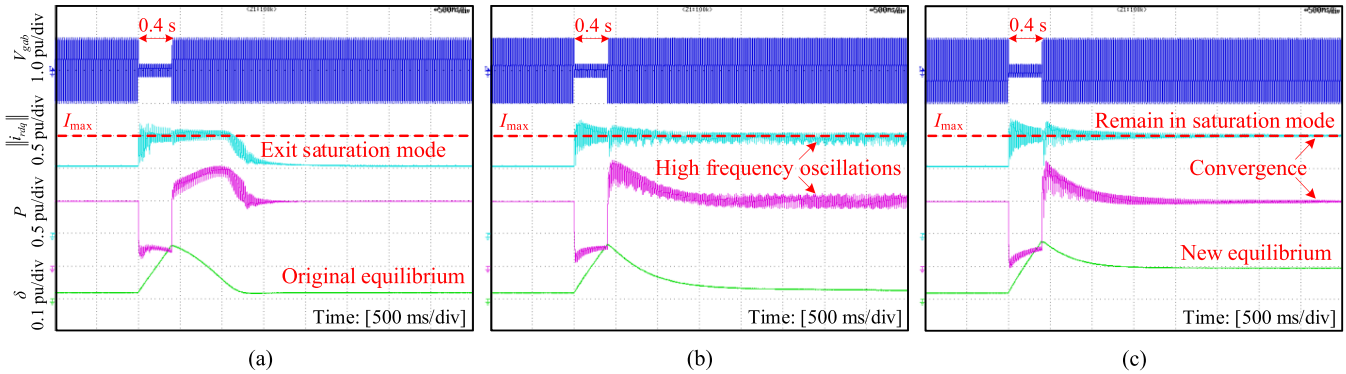


Fig. 3. Simulation results when the grid voltage drops to 0.2 p.u. (a) *Case 1:* $\varphi = -0.4$ rad. (b) *Case 2:* $\varphi = -1.1$ rad. (c) *Case 3:* $\varphi = -1.4$ rad.

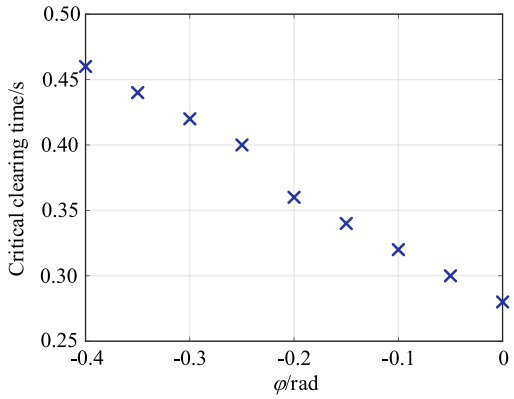


Fig. 4. Variation of the critical clearing time with respect to the SCA.

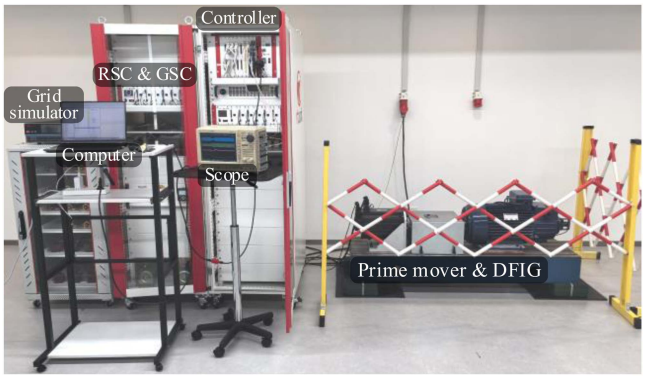


Fig. 5. Full hardware experimental platform.

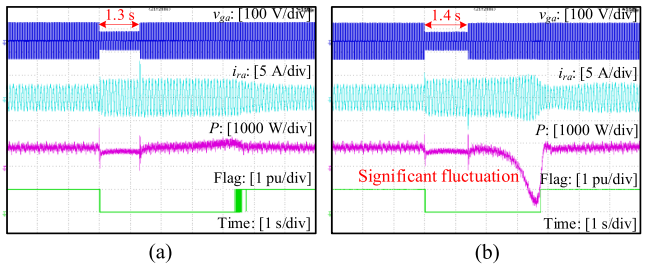


Fig. 6. Experimental results of GFM-DFIG equipped with circular limiter when the grid voltage drops to 0.5 p.u. (a) Fault duration of 1.3 s. (b) Fault duration of 1.4 s.

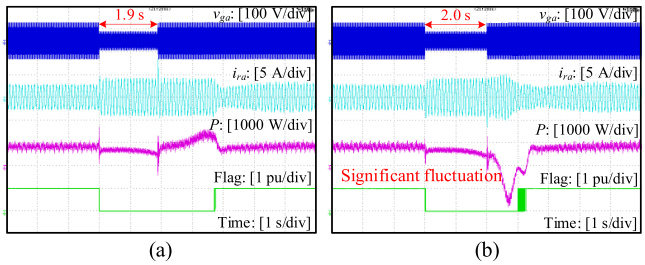


Fig. 7. Experimental results of GFM-DFIG equipped with priority-based limiter with $\varphi = -0.7$ rad when the grid voltage drops to 0.5 p.u. (a) Fault duration of 1.9 s. (b) Fault duration of 2.0 s.

remains locked in the saturation mode even after fault clearance. Three different operating conditions are summarized in Table II.

## V. Experimental Verification

### A. Control Hardware-in-Loop Simulations

Simulations based on a control hardware-in-loop platform are conducted to validate the theoretical analysis. The DFIG and corresponding converter, as shown in Fig. 1, are simulated in the Typhoon HIL 602+ environment with a time step of 1 $\mu$s. The control strategies are implemented on the TMS320F28335 DSP accompanied by an field programmable gate array (FPGA) control board. Under different SCA selections, simulation results when the grid voltage drops to 0.2 p.u. are shown in Fig. 3.

As shown in Fig. 3(a), GFM-DFIG does not exit the current limiting state immediately upon grid voltage restoration. This corresponds to the continuously decreasing operating point indicated by the green arrow, as shown in Fig. 2(b), before entering the yellow region. Subsequently, $\delta \in \Omega_2$ and $\delta \notin \Omega_1$ hold, allowing the system to restore normal operation and return to its original equilibrium point. It can be observed that GFM-DFIG achieves fault ride-through in this case with the RSC output current effectively constrained.

As illustrated in Fig. 3(b), the operating point enters the region corresponding to $\delta \in \Omega_2 \cap \Omega_1$ with $\varphi = -1.1$ rad. Thereafter, GFM-DFIG experiences high-frequency oscillations introduced by the priority-based current limiter, which severely jeopardizes transient stability of the system.

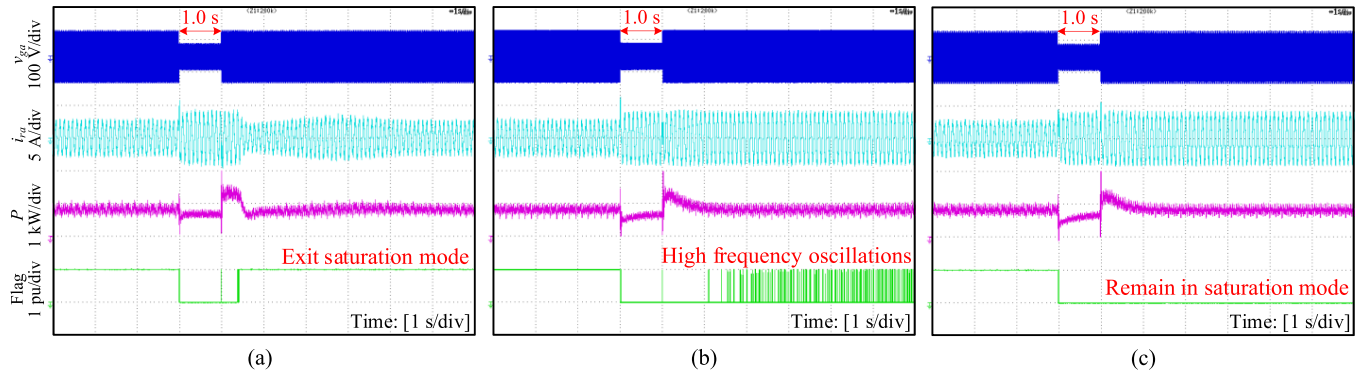


Fig. 8. Experimental results of GFM-DFIG equipped with priority-based limiter. (a) *Case 1:* $\varphi = -0.7$ rad. (b) *Case 2:* $\varphi = -1.2$ rad. (c) *Case 3:* $\varphi = -1.4$ rad.

TABLE II
SUMMARY OF DIFFERENT TRANSIENT BEHAVIORS

| Case number | Regions entered in Fig. 2 | Post-fault behaviors in Fig. 3 |
|---|---|---|
| 1 | Yellow ($\delta \in \Omega_2$ and $\delta \notin \Omega_1$) | Exit saturation mode |
| 2 | Pink ($\delta \in \Omega_2 \cap \Omega_1$) | High frequency oscillations |
| 3 | Red line (SEP in saturation state) | Remain in saturation mode |

As shown in Fig. 3(c), when $\varphi = -1.4$ rad is applied, GFM-DFIG stabilizes at an abnormal equilibrium point in the current limiting state before entering the region corresponding to the exit from the saturation mode. Although DFIG system remains synchronized with the grid, successful fault recovery is prevented by the continuous activation of the current limiter.

The variation of the system's critical clearing time with respect to the SCA is illustrated in Fig. 4. It can be observed that a smaller SCA enhances the fault ride-through capability of the DFIG. Therefore, to improve the transient performance of the system while avoiding undesirable postfault behaviors, it is advisable to select the smallest possible SCA, provided that successful current limitation withdrawal is ensured.

### B. Full Hardware Experiments

To further compare the transient performance of different current limiters, full hardware experiments are conducted using the experimental platform, as shown in Fig. 5. The back-to-back converter and its associated controllers are implemented on the Rtunit RTU-BOX206 platform, with the output from GFM-DFIG linked to an Actionpower PRE2020S grid simulator. Detailed experimental parameters are given in Table III.

Fig. 6 presents the experimental results of GFM-DFIG equipped with circular limiter when the grid voltage drops to 0.5 p.u. Flag = 1 indicates normal operation, while Flag = 0 signifies fault current limiting. As shown in Fig. 6(b), when the fault duration is 1.4 s, the active power output of the DFIG experiences significant fluctuations after the grid voltage is restored. It is important to note that during the transient phase, the reverse flow of active power may pose a risk of damaging the generator system, which is unacceptable in practical applications [13].

TABLE III
DETAILED EXPERIMENTAL PARAMETERS

| PARAMETER | Value | PARAMETER | Value |
|---|---|---|---|
| $V_g$, Grid voltage | 82 V | $\omega_1$, Rated angular frequency | 100π rad/s |
| $P_{nom}$, Rated power | 1000 W | $P^{ref}$, Power reference | 0.8 p.u. |
| $K_e$, Turn ratio | 0.36 | $L_s$, Stator inductance | 3.49 p.u. |
| $n_p$, Pairs of poles | 3 | $L_r$, Rotor inductance | 3.55 p.u. |
| $R_s$, Stator resistance | 0.07 p.u. | $L_m$, Magnetizing inductance | 3.42 p.u. |
| $R_r$, Rotor resistance | 0.06 p.u. | $E$, Voltage reference | 1.05 p.u. |
| $R_v$, Virtual resistance | 0.2 p.u. | $L_v$, Virtual inductance | 0.2 p.u. |
| $K_p$, Droop gain | 0.01 p.u. | $I_{max}$, Maximum current | 1.22 p.u. |

Therefore, when using the circular current limiter, the critical clearing time of GFM-DFIG is 1.3 s.

Fig. 7 presents the experimental results of GFM-DFIG equipped with priority-based limiter when the grid voltage drops to 0.5 p.u., where the SCA is set at $\varphi = -0.7$ rad. During the fault period, the rotor current is effectively limited. It can be observed that the critical clearing time of the system is extended to 1.9 s, which represents a 46% increase compared to the result obtained when using the circular limiter. Therefore, GFM-DFIG with the priority-based limiter selected in this study demonstrates the enhanced fault ride-through capability.

However, the additional control degree of freedom provided by the SCA must be carefully adjusted. This is necessary to avoid the occurrence of undesirable high-frequency oscillations and sustained saturation, as shown in Fig. 8(b) and (c). To theoretically investigate the above issue, the impact of the SCA on the system's transient performance is quantitatively analyzed, which can guide the selection of current-limiting parameters for improving the robustness of GFM-DFIG.

## VI. Conclusion

This letter investigates the postfault transient stability of GFM-DFIG equipped with a priority-based limiter. Since an asynchronous machine serves as an intermediary between the control objective and its implementation, the dynamics of the voltage controller are considered when establishing transient models under normal operation and current-limiting conditions.

According to the control mode switching logic, theoretical analysis reveals three transient behaviors of GFM-DFIG after fault recovery. In addition to the withdrawal of current limitation, unexpected high-frequency oscillations on both the stator and rotor sides caused by the repeated switching of operating modes, and remaining locked in saturation due to stabilization at an abnormal equilibrium, might also occur. After selecting the SCA based on the theoretical analysis presented in this letter, better transient performance can be achieved compared to existing current limitation control techniques, while the effective fault current constraint and the robustness of GFM-DFIG are also guaranteed.

## References

[1] D. Zhu, Z. Wang, Y. Ma, J. Hu, X. Zou, and Y. Kang, "Hybrid LVRT control of doubly-fed variable speed pumped storage to shorten crowbar operational duration," *IEEE Trans. Power Electron.*, vol. 39, no. 11, pp. 14192–14203, Nov. 2024.

[2] H. Li, B. Hu, H. Nian, Y. Liao, L. Xiong, and Z. Liang, "Impedance characteristic analysis and phase-locked angle feedforward-based stability improvement for LCC-HVDC in sending ac grid," *IEEE Trans. Sustain. Energy*, vol. 16, no. 1, pp. 588–600, Jan. 2025.

[3] X. Xiong, C. Wu, B. Hu, D. Pan, and F. Blaabjerg, "Transient damping method for improving the synchronization stability of virtual synchronous generators," *IEEE Trans. Power Electron.*, vol. 36, no. 7, pp. 7820–7831, Jul. 2021.

[4] L. Zhan, B. Hu, L. Chen, Y. Liao, M. Li, and H. Nian, "Transient stability enhancement of current limited-GFM inverters based on varying virtual impedance," *IEEE Trans. Ind. Electron.*, vol. 71, no. 12, pp. 15946–15958, Dec. 2024.

[5] Z. Li, Z. Xie, S. Xu, and X. Zhang, "Improving transient stability of grid-forming DFIG based on enhanced hybrid synchronization control," *IEEE Trans. Ind. Electron.*, vol. 71, no. 12, pp. 15881–15894, Dec. 2024.

[6] L. Huang, H. Xin, Z. Wang, L. Zhang, K. Wu, and J. Hu, "Transient stability analysis and control design of droop-controlled voltage source converters considering current limitation," *IEEE Trans. Smart Grid*, vol. 10, no. 1, pp. 578–591, Jan. 2019.

[7] B. Fan and X. Wang, "Fault recovery analysis of grid-forming inverters with priority-based current limiters," *IEEE Trans. Power Syst.*, vol. 38, no. 6, pp. 5102–5112, Nov. 2023.

[8] *IEEE Standard for Interconnection and Interoperability of Inverter-Based Resources (IBRs) Interconnecting with Associated Transmission Electric Power Systems.*, IEEE Standard 2800-2022, 2022.

[9] E. Rokrok, T. Qoria, A. Bruyere, B. Francois, and X. Guillaud, "Transient stability assessment and enhancement of grid-forming converters embedding current reference saturation as current limiting strategy," *IEEE Trans. Power Syst.*, vol. 37, no. 2, pp. 1519–1531, Mar. 2022.

[10] D. Zhu, Y. Ma, X. Li, L. Fan, B. Tang, and Y. Kang, "Transient stability analysis and damping enhanced control of grid-forming wind turbines considering current saturation procedure," *IEEE Trans. Energy Convers.*, early access, Aug. 13, 2024, doi: 10.1109/TEC.2024.3442925.

[11] Y. Ma, D. Zhu, Z. Zhang, X. Zou, J. Hu, and Y. Kang, "Modeling and transient stability analysis for type-3 wind turbines using singular perturbation and Lyapunov methods," *IEEE Trans. Ind. Electron.*, vol. 70, no. 8, pp. 8075–8086, Aug. 2023.

[12] S. Chen et al., "Transient stability analysis and improved control strategy for dc-link voltage of DFIG-based WT during LVRT," *IEEE Trans. Energy Convers.*, vol. 37, no. 2, pp. 880–891, Jun. 2022.

[13] L. Zhan, B. Hu, L. Chen, S. Zhang, Z. Zhang, and H. Nian, "Transient stability analysis of grid-forming DFIG equipped with circular current limiter," *IEEE Trans. Ind. Electron.*, early access, Apr. 28, 2025, doi: 10.1109/TIE.2025.3559957.